2003

Numerical Investigation of Transonic Flutter and Modeling of Wind Tunnel Interference Effects

Castro, B.M.

NUMERICAL INVESTIGATION OF TRANSONIC FLUTTER AND MODELING OF WIND TUNNEL INTERFERENCE EFFECTS

Breno M. Castro, Kevin D. Jones and Max F. Platzer
Naval Postgraduate School
Monterey, CA USA
bmcastro@nps.navy.mil, jones@nps.navy.mil, platzer@nps.navy.mil

Stefan Weber
MTU Aero Engine Design, Inc.
Rocky Hill, CT USA
stefan.weber@muc.mtu.de

John A. Ekaterinaris
Foundation for Research and Technology Hellas
Heraklion, Greece
ekaterin@iacm.forth.gr

Abstract

Computational investigations of transonic limit-cycle flutter of the NLR 7301 supercritical airfoil using a thin-layer Navier-Stokes solver are presented. Results are given showing the effect of turbulence and transition modeling and of wind-tunnel interference. Comparisons are made with the experiments of Schewe and Deyhle. The results show that both viscous effects and wind tunnel interference effects are significant, and need to be correctly modeled in the computations.

1. Introduction

It is the objective of this paper to summarize our computational investigations of transonic limit-cycle oscillation (LCO) flutter of the NLR 7301 supercritical airfoil using a thin-layer Navier-Stokes solver. To this end, we first discuss the role of turbulence and transition modeling and

of wind tunnel wall interference to obtain agreement with the measured *steady-state* aerodynamic characteristics and then proceed to the analysis of the LCO flutter phenomenon. Our emphasis is on highlighting the major physical aspects. For computational details we refer to Weber et al., 2001, Castro et al., 2002 and Castro et al., 2001.

2. Basic Approach

The unsteady, compressible, two-dimensional, thin-layer Navier-Stokes equations in the strong conservation law form are used. The numerical algorithm was developed and validated in Ekaterinaris et al., 1994, Ekaterinaris et al., 1998 and Ekaterinaris and Menter, 1994. It performs time marching with the implicit, factorized, iterative Beam and Warming algorithm. The inviscid fluxes are evaluated using Osher's third-order upwind-biased scheme. Linearization of the left-hand side is performed by evaluating the flux Jacobian matrices with the Steger-Warming flux-vector splitting. The viscous fluxes are computed with second-order central differences. Furthermore, a standard minmod TVD scheme is used to eliminate numerical oscillations at flow discontinuities, such as shocks. Time accuracy is improved by performing Newton subiterations to convergence within each physical time step. These subiterations minimize the linearization and factorization errors and help drive the left-hand-side residuals to zero within each physical time step. This Navier-Stokes solver has been tested extensively in a variety of unsteady subsonic and transonic flow studies, such as by Ekaterinaris et al., 1994. The transitional flow region was computed with an effective eddy viscosity scaled by the intermittency function proposed by Gostelow et al., 1996. A breakdown-rate parameter of 1.0 was chosen and the transition onset was either predicted by the Michel criterion (Michel, 1957) or by specification as an input parameter.

3. Steady-state Computations

In a first series of computations (Weber et al., 2001), 221×91 and 337×91 point grids were used, and the outer boundaries of the computational domain were put at 20 chord lengths. Corrections for the effect of the wind tunnel walls in the experiment of Schewe and Deyhle, 1996, were attempted by progressively varying both the free-stream speed and the angle of incidence until the computed steady surface pressure distributions matched the experimental values as closely as possible. This led to the choice of $M_\infty = 0.753$ and $\alpha = -0.08$ and the results shown in Fig. 1.

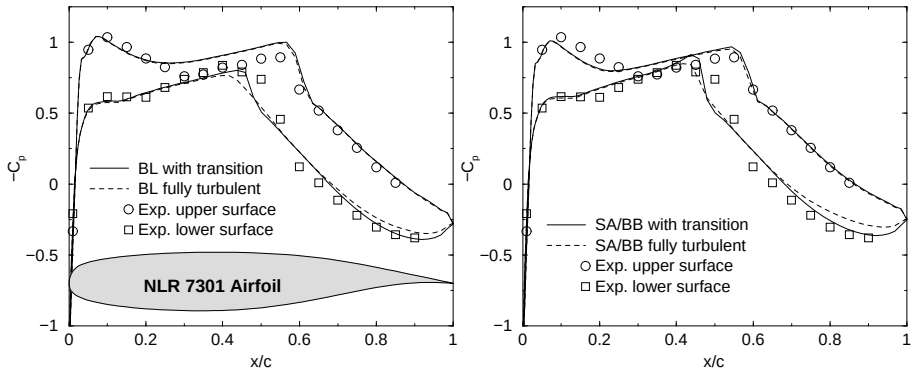

Figure 1. Steady pressure distributions for BL, SA and BB turbulence models for unbounded flow at corrected conditions: $M_\infty = 0.753$, $\alpha = -.08$ degrees.

The comparisons between the experiment and the computations using the Baldwin-Lomax (BL), Spalart-Allmaras (SA) and Baldwin-Barth (BB) turbulence models, with and without transition are shown. The incorporation of transition modeling is seen to improve the agreement on the pressure surface, whereas use of the SA or BB models leads to significant improvement on the suction surface. Transition onset was assumed to occur at 3% chord length on the suction surface. Michel's criterion was used on the pressure surface and gave the transition onset at 44% chord length. No laminar separation bubbles were predicted in any of the computations.

In a second series of computations (Castro et al., 2002) the presence of the wind tunnel walls was explicitly included using a *blocked-porous* scheme. The effect of tunnel porosity was modeled by prescribing solid and porous conditions on blocks of the wall, where inviscid conditions are applied on the solid part and outflow conditions are applied on the porous part by extrapolating the flow quantities from the interior points near the holes. The grid was constructed with an approximately constant grid spacing in the streamwise direction so that a porosity of 25% was achieved, for example, using a three-cell block of solid wall and a one-cell block that was a hole. Using the nominal wind tunnel test conditions, namely $M_\infty = 0.768$, $\alpha_0 = 1.28$ and Re=1.727×10^6, the pressure distributions shown in the left side of Fig. 2 were obtained using a solid wall and a wall with 50% porosity (alternating 4 solid wall cells with 4 hole cells). It is seen that this type of modeling of the wind tunnel walls yields a significant improvement over the computations without tunnel walls.

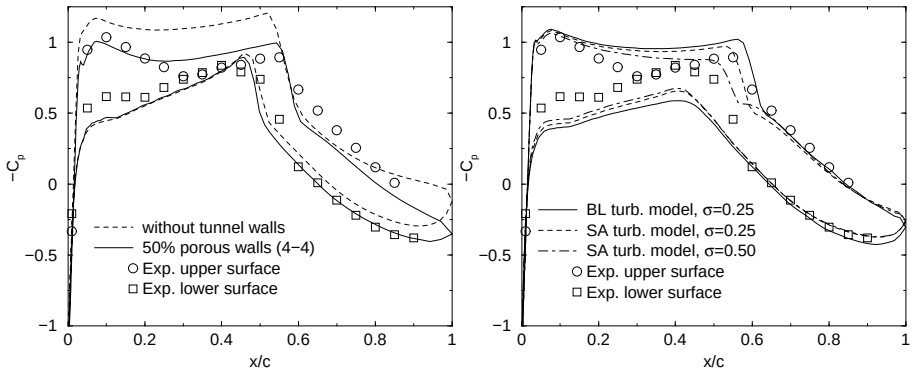

Figure 2. Steady surface pressure comparisons for the blocked-porous (left) and continuously-porous (right) boundary conditions at the experimental flow conditions: $M_\infty = 0.768$, $\alpha = 1.28$ degrees.

In a third series of computations the *blocked-porous* scheme was replaced by a *continuously-porous* scheme. The more general porous wall boundary condition described by Mokry et al., 1983,

$$\frac{w}{U_\infty} = \sigma \frac{p - p_{plenum}}{\rho_\infty U_\infty^2} \tag{1}$$

was implemented, where σ is the porosity parameter. For $\sigma = 0$ the normal velocity w at the wall is zero and hence the wall is solid and can be treated with either an inviscid wall condition by prescribing the flow tangency condition or as a viscous wall condition by prescribing the no-slip condition. Both conditions were investigated by Castro et al., 2001. The effect of two values of the porosity parameter, 0.25 and 0.5, on the computed pressure distributions, using the viscous wall condition and the nominal wind tunnel test conditions are shown in the right side of Fig. 2. As in the previous wall interference calculation the influence of the tunnel walls is seen to be quite significant. The agreement with the experiment is quite good on the suction surface, but there is a larger discrepancy on the pressure surface over the forward part of the airfoil than in the previous wall interference calculation. Nevertheless, both wall interference calculations show that the wall interference effects are non-negligible.

4. Flutter Computations

Flutter calculations were performed using the three above described steady-state results as starting conditions for the aeroelastic analysis. In the experiments (Schewe and Deyhle, 1996, Knipfer et al., 1998) the free-

stream Mach number was 0.768 and limit-cycle oscillations in pitch and plunge were found. The details of the experimental conditions and of the aeroelastic analysis are given in Weber et al., 2001, Castro et al., 2002 and Castro et al., 2001 and, therefore, will not be repeated here. Suffice it to note that two-degree-of-freedom pitch-plunge flutter was analyzed and the time integration of the resulting system of two coupled, second-order, ordinary differential equations was performed using the first-order accurate explicit Euler scheme.

In this paper we concentrate on comparing the results obtained by the unbounded flow assumption and by the two wind tunnel wall analyses using different treatments of the porous wall condition. This comparison is summarized in Table 1 where the measured and computed average incidence angle, the maximum half-amplitude of the pitch oscillation, the maximum half-amplitude of the plunge amplitude, the flutter frequency, and the phase angle between pitch and plunge are listed. It is seen that the unbounded flow calculations are in close agreement with the measured frequency and phase angle, but the computed amplitudes are an order of magnitude larger. Incorporation of wall interference yields significantly smaller amplitudes and hence closer agreement with the experiment, albeit with some deterioration of the computed frequency and phase angle values. This improvement is achieved by imposing either a 50% porosity with alternating 4 solid wall and 4 hole cells or with a porosity parameter of 0.25 and viscous wall conditions. However, imposition of the inviscid wall condition for $\sigma = 0.25$ suppresses flutter entirely using both the Spalart-Allmaras or Baldwin-Lomax turbulence model.

Table 1. Flutter Results

Method	$\overline{\alpha}$ *(deg)*	$\hat{\alpha}$ *(deg)*	$\hat{h}$ *(mm)*	f (Hz)	ϕ (deg)
experimental[a]	1.28	0.18	0.65	32.8	177
Spalart-Allmaras[b]	0.07	3.78	11.1	32.3	172
Spalart-Allmaras[c]	1.24	0.78	2.90	36.7	149
Spalart-Allmaras[d]	1.19	0.00	0.00	-	-
Spalart-Allmaras[e]	1.15	1.70	4.68	34.5	165
Baldwin-Lomax[d]	1.11	0.00	0.00	-	-
Baldwin-Lomax[e]	0.98	1.79	5.00	34.6	165

[a] without wind-tunnel corrections (Schewe and Deyhle, 1996).
[b] fully turbulent unbounded computation (Weber et al., 2001).
[c] 4-4 blocked porous boundary (Castro et al., 2002).
[d] continuous porous, inviscid wall; $\sigma = 0.25$ (Castro et al., 2001).
[e] continuous porous, viscous wall; $\sigma = 0.25$ (Castro et al., 2001).

This insensitivity to the turbulence model is also seen for the viscous wall conditions where the Spalart-Allmaras and Baldwin-Lomax models yield quite comparable results. Variation of the porosity, on the other hand, has a large influence for low values of the porosity parameter, as shown in the left side of Fig. 3. In fact, for values less than 0.12 flutter is completely suppressed, and there is a large sensitivity for values between 0.12 and 0.25. There is an additional strong sensitivity to the wind-tunnel height, or the *solid-blockage*, as shown in the right side of Fig. 3. The experiment had $H/c = 3.33$, where LCO is predicted, but for larger values of H/c the motion is damped.

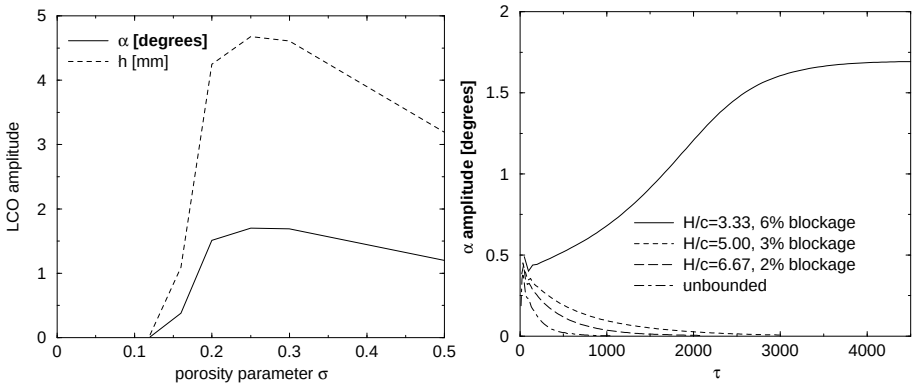

Figure 3. Flutter sensitivity to σ and solid blockage.

Additional information about the type of flow that leads to limit-cycle flutter can be gleaned from Fig. 4 where the flow field changes are shown during one oscillation cycle. It is seen that there are large changes in shock strength and position on both suction and pressure side, including shock induced flow separation during part of the cycle. The major nonlinear effects occur, as expected, for the highest incidence angle.

5. Summary

The Reynolds-averaged Navier-Stokes computations of limit-cycle flutter of the NLR-7301 airfoil show that viscous and wind-tunnel interference effects, including both porosity and blockage factors, are significant. Two different techniques of modeling the porous wind tunnel walls were developed. Steady results showed a dependence on transition location. Further work is required to assess the sensitivity of this type of flutter to tunnel interference effects and transition modeling.

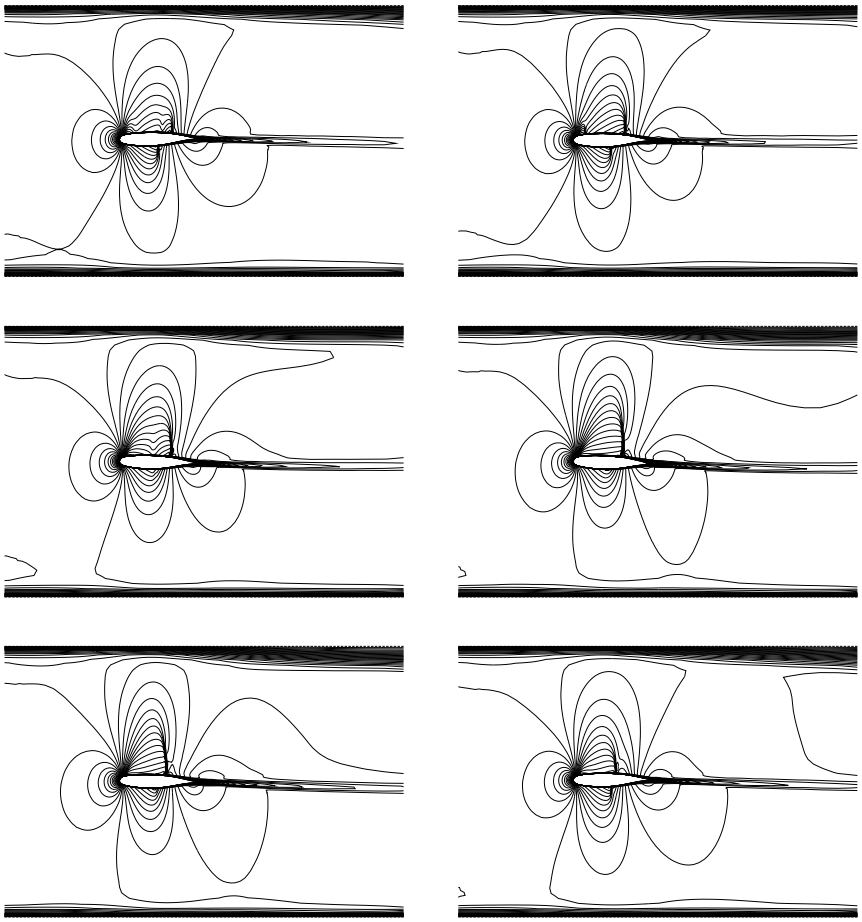

Figure 4. Mach contours at ϕ=0, 60, 120, 180, 240 and 300 degrees.

References

Castro, B. M., Ekaterinaris, J. A., and Platzer, M. F. (2002). Navier-Stokes analysis of wind-tunnel interference on transonic flutter. *AIAA Journal*, 40:1269–1276.

Castro, B. M., Jones, K. D., Ekaterinaris, J. A., and Platzer, M. F. (2001). Analysis of the effect of porous wall interference on transonic airfoil flutter. AIAA Paper No. 2001-2725.

Ekaterinaris, J. A., Cricelli, A. S., and Platzer, M. F. (1994). A zonal method for unsteady, viscous, compressible airfoil flows. *Journal of Fluids and Structures*, 8:107–123.

Ekaterinaris, J. A. and Menter, F. R. (1994). Computation of oscillating airfoil flows with one- and two-equation turbulence models. *AIAA Journal*, 32:2359–2365.

Ekaterinaris, J. A., Sorensen, N. N., and Rasmussen, F. (1998). Numerical investigation of airfoil dynamic stall in simultaneous harmonic oscillatory and translatory motion. *ASME Journal of Solar Energy Engineering*, 120:75–83.

Gostelow, J. P., Melwani, N., and Walker, G. J. (1996). Effects of a streamwise pressure gradient on turbulent spot development. *Journal of Turbomachinery*, 118:737–747.

Knipfer, A., Schewe, G., and Wendt, V. (1998). Numerische und experimentelle untersuchungen an einem schwingenden NLR7301-profil in transsonischer stroemung, teil 1: Flattern und erzwungene schwingungen. DLR Bericht IB 232-98 J 05.

Michel, R. (1957). Etude de la transition sur les profiles d'aile. ONERA Report 1/1578A.

Mokry, M., Chan, Y. Y., and Jones, D. J. (1983). Two-dimensional wind tunnel wall interference. AGARDograph No. 281.

Schewe, G. and Deyhle, H. (1996). Experiments on transonic flutter of a two-dimensional supercritical wing with emphasis on the non-linear effect. Proceedings of the Royal Aeronautical Society Conference on Unsteady Aerodynamics, London.

Weber, S., Jones, K. D., Ekaterinaris, J. A., and Platzer, M. F. (2001). Transonic flutter computations for the NLR 7301 supercritical wing. *Aerospace Science & Technology*, 5:293–304.